PREDICTING ION EXCHANGE BEAD RISE DURING BACKWASH FLOW

By

SANKET KULKARNI

Bachelor of Chemical Engineering

Vishwakarma Institute of Technology

University of Pune

Pune, Maharashtra, India

2007

Submitted to the Faculty of the
Graduate College of the
Oklahoma State University
in partial fulfillment of
the requirements for
the Degree of
MASTER OF SCIENCE
July, 2012

PREDICTING ION EXCHANGE BEAD RISE

DURING BACKWASH FLOW

Thesis Approved:

Dr. Gary L. Foutch

Thesis Adviser

Dr. Sundar Madihally

Dr. Josh Ramsey

Dr. Sheryl A. Tucker

Dean of the Graduate College

TABLE OF CONTENTS

LIST OF TABLES

Table Page

LIST OF FIGURES

Table Page

NOMENCLATURE

Ar	Archimedes number
C_D	Drag coefficient
D	Diameter of column, m
d_p	Diameter of particle, m
F_A	Force on an accelerated body, N
F_B	Buoyant force on particle
F_D	Drag force on particle, N
F_{DS}	Drag force on a single particle in an infinite expanse of fluid, N
F_G	Gravitation force, N
Fr	Froude Number
g	Acceleration due to gravity, m/s^2
Ga	Galileo number
h	Height of bed, m
m_p	Mass of resin particle, kg
Re	Reynolds number
u_f	Superficial velocity of fluid based on an empty column, m/s
u_p	Velocity of particle, m/s
u_t	Terminal velocity of particle, m/s
δ	Boundary layer thickness
δ_0	Boundary layer thickness parameter used by Abraham (1970)

ε	Void fraction of bed
θ_s	Angle of boundary layer separation
ρ	Density of resin particle, kg/m^3
ρ_f	Density of fluid, kg/m^3
ρ_p	Density of particle, kg/m^3
μ	Kinematic viscosity, Ns/m^2

CHAPTER I

INTRODUCTION

ULTRA PURE WATER

Water is one of the primary reasons why life exists on Earth. With man's need to innovate, we have found countless applications for water. It is a transport medium, an indispensible ingredient in the food and beverage industry and a process material in the power industry. Due to its unique properties, water is easy to use, purify and reuse. Because of its thermodynamic properties and relatively low cost it is a working fluid in power cycles. Today, water quality is equally important as its availability with much research done on water purification. Ultra Pure Water (UPW) is an integral part of the power, pharmaceutical and microelectronics industries. Thus, innovation in these industries is complimented with a breakthrough in the water purification technology.

The choice of water treatment technology depends on the process specifications and cost. The most widely used UPW technologies include

1. Ion Exchange

2. Microfiltration

3. Reverse Osmosis (RO)

4. Vibratory Shear Enhanced Processing

The comparison between RO and Ion Exchange has been a subject of numerous studies. RO is more expensive because of the membrane that needs to be replaced periodically. RO also requires more pumping energy than ion exchange and is less desirable if pumping costs are higher. Although RO does not involve regeneration costs, membrane cleaning is an inherent cost. RO units are rated for lower temperatures around 25°C while ion exchange units can run at higher temperatures up to 50˚C. RO also requires a more rigorous pretreatment when compared with ion exchange. RO systems run continuously without a downtime for regeneration while ion exchangers need to be regenerated periodically. Ion exchange is preferred technology in the power industry.

Due to the nature of the steam cycle, some accumulation of impurities is anticipated in the process water within the plant. Such impurities may corrode vital equipment and lead to downtime for maintenance. Removing the impurities reduces equipment damage and improves the process efficiency. UPW is used in the power industry for this purpose. In the power industry Mixed Bed in Exchange (MBIE) technology produces UPW make-up water, polishes condensate and cleans reactor water. The MBIE bed removes ionic impurities and purifies water to parts per billion (ppb) or parts per trillion (ppt) levels.

ION EXCHANGE

Ion Exchangers have been defined as insoluble solid materials which carry exchangeable cations and anions" (Helfferich 1995) and the reversible process of exchange of ions between the exchangers and the liquid phase is defined as ion exchange. This interchange of ions is stoichiometric. The exchangers that carry positively charged ions are called cations and those carrying negatively charged ions are called anions. Ion exchange units typically are vertical pressure vessels and their size depends on the flow rates required, amount of resin used and expected bed expansion during bed operation (Owens 1995). Due to its reversible nature, ion exchange has been a preferred method of water purification.

MIXED BED ION EXCHANGE

MBIE was first proposed as Monobed Deionization (Kunin and McGarvey 1951) in which water was passed through a single bed that contained an intimate mixture of cationic and anionic resins. Kunin and McGarvey described a single MBIE bed as "a large number of alternating single columns in series". This arrangement reduces the increased capital cost involved in installing and maintaining separate columns for water treatment. The ratio in which the two resins are mixed depends on the applications. Thus, the premise of this technology dictates that the cationic and anionic resins be different in particle size and density for easy separation and regeneration.

Prior to operation, the bed is charged with regenerated cationic and anionic resin in the hydrogen and hydroxyl forms respectively. Depending on the

resin polymer and the degree of crosslinking, different ion selectivity values are available. The selectivity coefficient of an ion is its relative affinity over hydrogen or hydroxyl ion. Figure 1 illustrates how a MBIE bed operates. As water with ionic impurities passes through the mixed bed, anions and cations in the influent stream react with the cationic and anionic resins releasing the hydrogen and hydroxyl ion. The released hydrogen and hydroxyl ions react to form water molecules. Using this parallel reaction scheme, the concentration of the impurities can be reduced to ppb or ppt levels. During operation, the active sites within the bed are depleted due to the reactions. This depletion continues along the length of the bed until all the resin is saturated and the bed is exhausted.

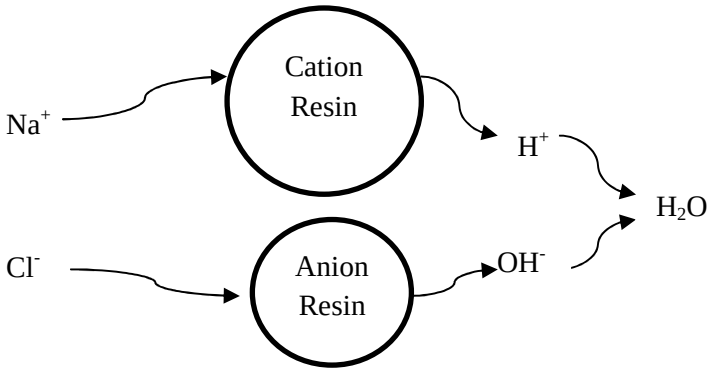

Figure 1.1 Removal of cation and anion from water using MBIE

IMPORTANCE OF RESIN SEPARATION STEP

For continued operation, the resin can be reused by regenerating the cationic resin with an acid and the anionic resin with a base. The regeneration step is done by transferring the two resin types into separate beds and treating them with their respective regenerant. The regeneration step however, requires

complete separation of the two resin types. Backwash is used to separate the intimate mixture of the cationic and anionic resins. During the backwash operation the bed is expanded to a particular height and allowed to settle. In consecutive backwashes an interface builds up in the mixed bed which separates the heavy cations to the bottom from the lighter anions on the top. During a backwash cycle the bed expands with the resin layers intact. The separation occurs when the bed is allowed to settle. Since the two resin particles have different diameters and densities they have different terminal settling velocities (a function of the density and diameter of the particle), thus separating them.

Due to the process nature, cross-contamination is a disadvantage. Cross contamination occurs due to inefficient separation of the two resin layers. As the ionic impurities get attached to the resin beads, they increase the density of the resin bead. Incomplete separation and therefore incomplete regeneration may increase the size distribution of the particles and result in cross contamination. The interfacial layer formed due to cross contamination is transferred to a different column where resins can be separated and transferred to their respective regeneration beds. This increases the operation cost. Another reason why cross contamination is undesirable is that it contributes to an increased initial loading fraction of the bed due to saturation of stray beads in contact with the wrong regenerant (e.g. sodium hydroxide on cation beads and acid on anion beads). A higher initial loading fraction leads to equilibrium leakage into the effluent water stream.

Thus, it is clear that resin separation is perhaps the most important step in regenerated bed operation. To achieve improved resin separation and reduce cross contamination we must study the backwash operation. By applying fundamental laws of physics and fluid mechanics we can investigate the forces acting on a particle during expansion and settling. By studying those two phenomena separately one can develop predictive models for the bed expansion.

This work addresses the basic phenomenon of resin backwash to better understand the bead rise during operation. The objectives of this study are:

1. Study the phenomenon of bead rise during backwash
2. Develop a mathematical model that predicts the bed height as a function of time and fluid velocity
3. Check effect of operational variables on model parameters

CHAPTER II

MOTION OF A SPHERICAL PARTICLE IN LIQUID FLUIDIZATION

Liquid-solid fluidization has been used in the process industry for a wide range of applications. They include catalytic cracking, crystallization, sedimentation, hydrometallurgical operations etc. From a research point of view, hydrodynamic behavior of different fluidized systems has been investigated. The terminal and minimum fluidization velocities and their relationship with the bed voidage have been parameters of particular interest.

The phenomenon of rise of a rigid spherical bead in a liquid medium can be treated as a liquid-solid fluidization problem. From a modeling perspective, liquid-solid fluidization is quite different from gas-solid fluidization. For liquid-solid fluidization, the bed starts expanding when the liquid enters at a velocity that is higher than the minimum fluidization velocity. The minimum fluidization velocity is the velocity at which the bed just begins to fluidize. Beyond this point the bed continues to expand due to the various dynamic forces acting on the particles and it behaves like a suspension. Throughout the expansion process each

particle moves independently and the whole bed expands uniformly as a homogeneous medium. This is known as “particulate fluidization” (Kwauk 1948).

In case of gas-solid fluidization, as the superficial velocity of the gas increases beyond the minimum fluidization velocity, the gas passes through bed in the form of bubbles or cavities which have no solids in them. This is due to erratic aggregation of particles accompanied by formation of channels through which the gas flows. Hence, this type of fluidization has been called “aggregative fluidization.”

Wilhelm and Kwauk suggested a criteria (Kwauk 1948; J. B. Romero 1962) based on the Froude number (*Fr*) as the minimum fluidization velocity to differentiate between these two extreme cases. According to their criteria, for $Fr > 1$ aggregative fluidization is observed and for $Fr < 1$, the fluidization is of particulate nature. This work assumes that bed expansion during backwash is particulate fluidization.

Didwania and Homsy (1981) conducted experiments and identified five distinct flow regimes in liquid fluidization: particulate (homogeneous fluidization), wavy flow, wavy flow with transverse structure, fine scale turbulent flow and bubbling regime. Particulate fluidization exists when the liquid velocity is between the minimum fluidization velocity and the transition velocity.

DRAG COEFFICIENT AND THE REYNOLDS NUMBER

Theoretical analysis of a multi-particle liquid-solid fluidized system has been a challenge to researchers. This can be attributed to the difficulty in

calculating the drag force acting on each particle due to its accelerated motion in the fluid. A way of simplifying the problem is to introduce a fudge factor called the "drag coefficient". The drag coefficient is a parameter that is used to express the effective drag force on a particle in terms of velocity. Understanding the relationship between the drag coefficient (C_D) and the particle Reynolds number (*Re*) is important in order to study the mechanics of fluidization. C_D is given by Stokes law in Equation (2.1). C_D is a function of the relative velocity of the particle with the fluid $(u_p - u_f)$ where u_f is the superficial velocity of the fluid, u_p is the velocity of the particle and *A* is the cross sectional area of the particle.

$$C_D = \frac{2F_D}{\rho\left(u_f - u_p\right)^2 A} \tag{2.1}$$

The drag coefficient accounts for all the frictional losses when solving the momentum balance equation for a system. In a bed expansion process, the particle velocity varies with time and therefore, transient velocity estimates are necessary when solving for bed expansion characteristics. The variations in particle velocity influence the particle Reynolds number for the system and therefore the effective drag on the particle. The C_D and *Re* are calculated at each time instance. By developing a generalized correlation, we get agreeable predictions of particle velocity. Researchers have spent the better part of the previous century trying to develop theoretically based expressions correlating C_D with *Re*. Most of the correlations in the literature are developed semi-empirically by curve fitting and reducing sum of square error with a set of experimental data. Also, a majority of the correlations were developed for free falling particles in liquid-solid systems

and reconciled to gas-solid systems (Mabrouk, Chaouki et al. 2007). Additionally, depending on the theoretical approach, they developed correlations based on unique assumptions. This resulted in considerable deviations among their predictions. Studies have been done on a variety of shapes including sphere, cylinder, and flat plate. This work includes correlations developed for rigid spherical particles.

$$\rho \frac{D}{Dt} u = -\nabla p + \mu \nabla^2 u \tag{2.2}$$

Equation 2.2 is the Navier-Stokes equation in vector notation. For creeping flow (very low velocities), the second term on the right hand side can be neglected. The drag force F_D in Equation 2.1 can be calculated by solving Equation 2.2 for this condition. This solution was first provided by Stokes (1851).

$$F_D = 3\pi\mu d u \tag{2.3}$$

The dimensionless drag coefficient C_D can be obtained by dividing the drag force F_D by the flow momentum $1/2\rho u^2$ and the projected area of the sphere A. Equation 2.4 is an alternate form of Stokes law.

$$C_D = \frac{F_D}{\frac{\pi \rho u^2 d^2}{8}} = \frac{24}{Re} \tag{2.4}$$

Stokes law (Equation 2.4), is one of earliest efforts to correlate the drag coefficient with the Reynolds number. This correlation however, is only applicable for Reynolds numbers less than one. In his review of C_D-Re

relationships, Kelbaliyev (2011) observes that most drag correlations for spheres ($Re \leq 500$) reduce to the form shown in Equation 2.5. In the generic form the parameters A and n are constants of various correlations reported in literature essentially making most of the equations modifications of the Stokes law. Table 2.1 lists some of the reported correlations in literature.

$$C_D = \frac{24}{Re}\left(1 + A\,Re^n\right) \tag{2.5}$$

Stokes assumed that the higher order velocity terms would have a negligible effect on the total drag on the sphere at low velocities. Oseen (1911) argued that for a wider application of the Stokes Law, the inertia terms must be included. Oseen (1911) assumed that the inertia forces would be of a lesser magnitude in the vicinity of the sphere. However, at a distance from the sphere those forces cannot be ignored and the higher order velocity terms ought to be included in the momentum balance (Brodkey 1967).

Table 2.1. Drag coefficient correlations

Source	Expressions	Conditions
Oseen (1911)	$C_D = \frac{24}{Re}\left(1 + \frac{3}{16}Re\right)$	$Re < 5$
Massey (1968)	$C_D = \frac{24}{Re}\left(1 + \frac{3}{16}Re\right)^{0.5}$	$Re < 100$
Schiller and Naumann (1933)	$C_D = \frac{24}{Re} + \frac{3.6}{Re^{0.313}}$	$0.1 < Re < 1000$
Lapple (1951)	$C_D = \frac{24}{Re}\left(1 + 0.125\,Re^{0.72}\right)$	$Re \leq 100$
Concha and Almendra (1979)	$C_D = 0.28\left(1 + \frac{9.06}{Re^{0.5}}\right)^2$	$0.1 < Re < 10^6$
Haider and Levenspiel (1988)	$C_D = \frac{24}{Re}\left(1 + 0.1806\,Re^{0.6459}\right) + \frac{0.4251}{1 + \frac{6880.9}{Re}}$	$Re < 2.6 \times 10^5$
Flemmer and Banks (1986)	$C_D = \frac{24}{Re}10^E$ where, $E = 0.261\,Re^{0.369} - 0.105\,Re^{0.431} - \frac{0.124}{1 + (\log_{10} Re)^2}$	$Re < 3 \times 10^5$

The total drag exerted by a fluid on a sphere can be considered as a sum of two components: friction drag and form drag. The former also known as viscous drag can be attributed to the viscous forces experienced by the sphere. Stokes Law accounts for the friction drag alone. The form or pressure drag is a function of the

size, shape and the pressure distribution on the surface of the sphere and can be estimated using Newton's drag law. At higher Reynolds number the form drag predominates and hence it cannot be neglected (Concha and Almendra 1979). The absence of form drag in Stokes law (Equation 2.4) can be considered as an additional explanation for its failure at higher Reynolds numbers ($Re \geq 1$)

Table 2.1 shows Oseen's modification of the Stokes drag law for a sphere (Equation 2.4). Massey (1968) further modified Oseen's expression and extended its applicability to $Re < 100$. Schiller and Naumann (Schiller and Naumann 1933) also modified Oseen's expression and further extended the Reynolds number range to 1000. Additional correlations based on the traditional Oseen's approximation were reported by Flemmer and Banks (Flemmer and Banks 1986). They proposed a complex C_D-Re correlation for a sphere applicable for Reynolds numbers up to 3×10^5.

Alternative methods for the estimation of terminal velocity have been suggested. One method used consistently suggests developing a C_D correlation with the Archimedes number (Ar). Since terminal velocity appears in both C_D and Re, an implicit expression of velocity is inconvenient to solve. To avoid this, it was suggested to develop C_D-Re^2 correlations. Such a correlation would be independent of the velocity term. Khan and Richardson (1987) used this method in their expressions.

$$C_D\,Re^2 = \frac{4d^3 g\rho(\rho_p - \rho)}{3\mu^2} = \frac{4}{3}Ar = \frac{4}{3}Ga$$

(2.6)

Equation 2.6 shows that the velocity term is eliminated. Also, the Galileo number (*Ga*) is the Archimedes number (*Ar*) when the particle density is equal to that of the fluid. Khan and Richardson (1987) expressed *Ar* as a function of the Reynolds number rather than the drag coefficient as it included only the physical properties of the particle and was independent of the settling velocity. Karamanev (1996) also based his correlation on *Ar*, however, his expression correlated C_D to *Ar* and not to *Re*.

VELOCITY VOIDAGE RELATIONSHIP

During the backwash operation, the fluid being pumped in the bed experiences resistance to flow due to the packing. Thus, the effective fluid velocity will be much lower than what it would have been if the bed was empty. This effective fluid velocity will be a function of the void fraction of the bed. It is therefore necessary to account for the change in the bed voidage as the bed expands for a liquid-solid system. A particle in such a suspension will experience a variety of external forces. Hence, it becomes increasingly difficult to account for the effects of the random interactions between the particles in an expanding bed. Experimental data reported in literature suggests that for a liquid fluidized bed the velocity-voidage relationship is independent of the total mass of the suspended solid particles.

Many equations have been developed relating the superficial fluid velocity to the terminal velocity using bed voidage. Courdec (1985) summarizes most of these expressions for fluidized beds. Courdec considers Richardson and Zaki (1954) to be the first important work in this approach. Richardson and Zaki developed an equation that related the ratio of the relative settling velocity and terminal settling velocity to the bed voidage. Their expression was successful in modeling a complex phenomenon with a simplistic expression and is widely cited. Equation (2.7) is the Richardson Zaki relation.

$$\frac{u}{u_t} = \varepsilon^n \tag{2.7}$$

This relation is entirely empirical derived from extensive experimental work. Richardson and Zaki investigated the dependence of settling velocity of spherical particles u with the bed void fraction ε. The form of Equation (2.6) was first used by Lewis and Bowerman (1952) to describe the velocity voidage relationship. However, Richardson and Zaki validated it with experimental data and found that the exponent n was a function of the particle Reynolds number and the particle to column diameter ratio d_p/D. The values of the parameter n as a function of Reynolds number reported by Richardson and Zaki are listed in Table 2.2.

Table 2.2 Values of parameter *n* in Richardson-Zaki equation

Reynolds number range	Value of parameter n
$0.2 < Re < 1$	$\left(4.35 + 17.5\frac{d_p}{D}\right)Re^{-0.03}$
$1 < Re < 200$	$\left(4.45 + 18\frac{d_p}{D}\right)Re^{-0.1}$
$200 < Re < 500$	$4.45\,Re^{-0.1}$

The drag force acting on a particle in a multiparticle system is affected by the voidage within the system. Thus for accurate prediction of the drag force, the bed voidage must be considered. Wen and Yu related voidage to a ratio of the drag force (F_D) acting on a particle in a multiparticle system and the drag force (F_{DS}) acting on a single particle in an infinite expanse of fluid. Wen and Yu (1966) presented such a ratio as shown in Equation 2.8 as the "voidage function".

$$\frac{F_D}{F_{DS}} = f(\varepsilon) \tag{2.8}$$

Many authors based their correlations on the voidage function to predict bed expansion. Yang and Renken (2003) for instance developed a new liquid particle interaction correlation that combined a C_D-Re^2 model with the voidage function.

Their model chooses a force ratio similar to that considered by Wen and Yu. They observed that the ratio of the effective gravitational force on the particle to the drag force is very sensitive to the parameter n of the Richardson-Zaki equation. They argued that the form ε^n for voidage function in Equation 2.8 is inappropriate. They developed an alternate functional relationship between the bed void fraction ε and Ar.

Another approach of modeling bed expansion reported in literature is expressing the bed expansion l_e/l in terms of individual variables such as particle sphericity φ, bed porosity ε, fluid viscosity μ, superficial bed velocity u, particle diameter and the particle and fluid densities ρ_p and ρ_f. Such a model was suggested by Dharmarajah and Cleasby (1986) where the power of each individual variable was found by regressing with experimental data. The powers in this least square model were later found by fitting them with extensive experimental data. This model was found to have a 9.5% minimum deviation. A similar but simpler backwash expansion model was also suggested by Sholji (1987).

CHAPTER III

MODEL DEVELOPMENT

The objective of this work is to develop a model that predicts the expansion of an ion exchange bed. This goal is achieved by studying an isolated single particle in the fluidized bed. The motion of this particle needs to be analyzed after the onset of fluidization. The distance it travels can be calculated as a function of time. By developing a velocity time relationship for the particle in component directions the height or the distance traveled by the particle can be calculated. A cylindrical coordinate system describes this problem adequately since the ion exchange bed used is a vertical cylindrical column. However, a simplifying assumption is made that the motion of the particle is only in the vertical *z* direction. Thus, the proposed model does not account for radial or phi displacement of the particle during its upward motion.

The particle of interest is assumed to be a rigid sphere wetted completely by the fluid. All the particles in the bed are assumed to have the exact same physical properties (density and mass) and dimension (diameter). . This is an excellent assumption for uniform bead resins (trade name Monosphere) that have very low variation in diameter. Also, properties of the particles are not affected by the fluid temperature. The average particle size (diameter) is assumed for calculations in the current model. Wall effects in a column are generally considered to contribute to particle retardation if the ratio of the particle to column diameter d_p/D is more than 0.05. In present work since this ratio is well below this value, the effects of the wall on the fluid flow profile are neglected.

MOMENTUM BALANCE ON A RISING SPHERICAL PARTICLE

A particle rising with the fluid will experience several external forces. These external forces will either decelerate or accelerate the particle depending on the direction they are acting. The net force on the particle will be the result of vector addition. By accounting for all forces and solving the momentum balance on the particle, the distance travelled by the particle can be predicted as a function of time.

The forces in the momentum balance equation (Equation 3.5) are:

1. Gravitational (F_G) - This force is due to the weight of the particle and acts in the negative z direction. Equation 3.1 gives the expression for F_G.

$$F_G = m_p g \tag{3.1}$$

2. Drag (F_D) - This is the frictional force acting on the particle due to its motion in the surrounding fluid. The expression for the drag force (Equation 3.2) has a modulus for the relative velocity to determine the direction of the drag force. When the fluid velocity is more than the particle velocity, F_D will act in the positive *z* direction.

$$F_D = \frac{\pi}{8} C_D \left(u_f - u_p\right)\left|u_f - u_p\right| d_p^2 \rho_f \tag{3.2}$$

3. Buoyant (F_B) - As per Archimedes principle, the buoyant force acting on the particle is equal to weight of the fluid displaced by the particle. F_B acts in the positive *z* direction.

$$F_B = m_f g \frac{\pi}{6} d_p^3 \rho_f g \tag{3.3}$$

4. Accelerated body (F_A) – This force is a function of the weight of the water displaced by the particle and it acts in a direction opposite to that of the buoyant force (negative *z* direction). It can be estimated using Equation 3.4.

$$F_A = \frac{1}{2} m_f g = \frac{\pi}{12} d_p^3 \rho_f \frac{du_p}{dt} \tag{3.4}$$

Lapple and Shepherd (1940) developed an equation of motion for the one-dimensional motion of a sphere moving in a stationary fluid. It was developed to model particle movement in commercial applications like aerosols, spray towers and drying. Ruckenstein (1964) modeled a particle settling in an infinitely long column. The directions of forces acting on a settling particle are exactly opposite to those for a rising particle. The drag force, F_D, on the particle is the most dominant. Thus, it contributes the most to the upward movement of the particle.

Additionally, the buoyant force F_B pushes the particle upward. F_B is accompanied by a reaction of the fluid to the particle due to its motion. This is the force F_A presented in the earlier list. Since it is a reaction to the particle's upward motion, F_A will have an opposite direction that is the negative z direction. Figure 3.1 presents a schematic of all the forces acting on the particle.

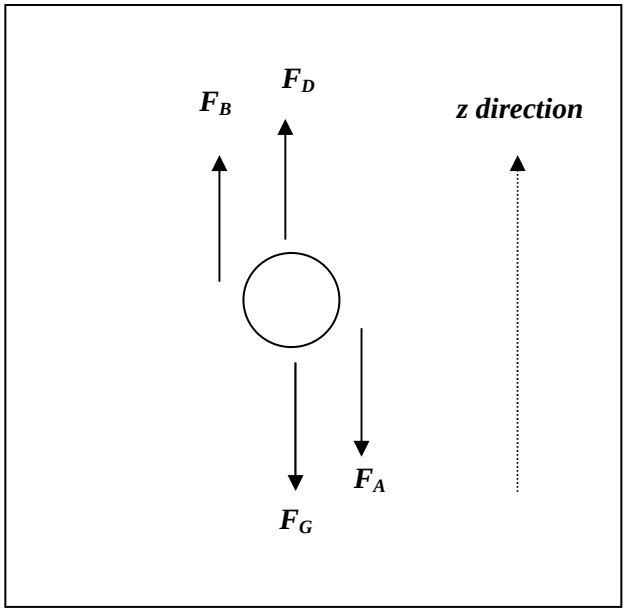

Figure 3.1 Forces acting on a rising spherical particle

Using Newton's law of motion, force balance on a rising particle is described in Figure 3.1 gives

$$F = m_p a = F_B + F_D - F_W - F_A \tag{3.5}$$

Equation 3.5 can be expanded as

$$m_p \frac{du_p}{dt} = m_f g \frac{\pi}{6} d_p^3 \rho_f g + \frac{\pi}{8}\left(u_f - u_p\right)\left|u_f - u_p\right| d_p^2 \rho_f C_D - m_p g - \frac{\pi}{12} d_p^3 \rho_f \frac{du_p}{dt}$$

F_B F_D F_W F_A

In the above expression m_p and m_f represent the mass of the particle and fluid respectively. They can be calculated by multiplying the volume of the spherical particle with the density. Substituting $m_p = (\pi d_p^3 \rho_p)/6$ and $m_f = (\pi d_p^3 \rho_f)/6$ and rearranging,

$$\left(\frac{\pi}{6} d_p^3 \rho_p g + \frac{\pi}{12} d_p^3 \rho_f\right)\frac{du_p}{dt} = \left(\frac{\pi}{6} d_p^3 \rho_f - \frac{\pi}{6} d_p^3 \rho_p\right) g + \frac{\pi}{8}\left(u_f - u_p\right)\left|u_f - u_p\right| d_p^2 \rho_f C_D$$

Now, dividing both sides by the volume of the spherical particle, $(\pi d_p^3)/6$ and rearranging,

$$\left(\rho_p + \frac{\rho_f}{2}\right)\frac{du_p}{dt} = \left(\rho_f - \rho_p\right) g + \frac{3\rho_f}{4 d_p}\left(u_f - u_p\right)\left|u_f - u_p\right| C_D$$

Dividing both sides of the equation by ρ_p,

$$\left(1 + \frac{\rho_f}{2\rho_p}\right)\frac{du_p}{dt} = \left(\frac{\rho_f}{\rho_p} - 1\right) g + \frac{3\rho_f}{4 d_p \rho_p}\left(u_f - u_p\right)\left|u_f - u_p\right| C_D$$

Substituting $\bar{\rho} = \rho_f / \rho_p$ and rearranging,

$$\frac{du_p}{dt} = \frac{1}{\left(1 + \frac{\bar{\rho}}{2}\right)}\left(\left(\bar{\rho} - 1\right) g + \frac{3\bar{\rho}}{4 d_p}\left(u_f - u_p\right)\left|u_f - u_p\right| C_D\right) \qquad (3.6)$$

Collecting terms and rewriting Equation 3.6

$$\frac{du_p}{dt} = \frac{B}{A} + \frac{C}{A}\left(u_f - u_p\right)\left|u_f - u_p\right| C_D \tag{3.7}$$

$$\frac{dh}{dt} = u_p \tag{3.8}$$

Where,

$$A = 1 + \frac{\bar{\rho}}{2}, B = \left(\bar{\rho} - 1\right)g$$

$$C = \frac{3\bar{\rho}}{4d_p}$$

PREDICTING BED EXPANSION

Equation 3.7 is the equation of motion of an isolated single spherical particle in a flowing stream. The velocity and the distance travelled or height of the particle can be calculated as a function of time by solving Equations 3.7 and 3.8. In order to predict the expansion of a fluidized bed, this model must be reconciled with a multiparticle system. While modeling expansion of a multiparticle packed bed, it is important to understand the effect of bed voidage on the fluid velocity. Prior to expansion, the non-fluidized bed will be highly dense depending on its static bed voidage. At the onset of fluidization when the bed starts expanding, the particles slowly move away from each other causing an increase the overall bed porosity and a decrease in the bed density. This results in

an increase in the fluid velocity due to reduced flow resistance. Yang and Renken (2003) developed a model for a fluidized bed. They chose to model the steady state condition of infinite expansion (ε =1) for an isolated particle. At such a condition, F_A is absent and the remaining three forces i.e. F_G, F_B and F_D balance each other. Yang and Renken included the voidage function in their expression. They combined the voidage function with the steady state force balance of a single particle and developed a model for the expansion of the entire bed.

Similarly, for the system of interest, the voidage function can be included in Equation 3.7 to describe the expansion of a fluidized bed. This modification has two advantages. Firstly, it accounts for the transient behavior of the bed during expansion, that is, the continuous increase in the bed porosity. Secondly, it accounts for the change in the buoyant force with the change in bed porosity. The density of the bed decreases as the bed expands. This decreases the cohesive force between neighboring particles and increases the effect of the buoyant force.

The voidage function accounts for the transient behavior of the bed through its dependence in the particle Reynolds number. The particle Reynolds number is a function of time and is calculated for each time value. In this work, the Richardson-Zaki correlation was used as the voidage function. This would change Equation 3.7 to

$$\frac{du_p}{dt} = \frac{B}{A} f(\varepsilon) + \frac{C}{A}\left(u_f - u_p\right)\left|u_f - u_p\right| C_D \tag{3.9}$$

where, for the range $1 < Re < 200$ (Richardson and Zaki 1954)

$$f(\varepsilon) = \varepsilon^n \quad \text{and} \quad n = \left(4.45 + 18\frac{d_p}{D}\right) Re^{-0.1} \tag{3.10}$$

Equations 3.8 and 3.9 form an initial boundary value problem, where boundary conditions depend on the bed geometry (initial height of bed). Height of the bed at a particular time instant can be calculated by solving Equations 3.9 and 3.8 simultaneously using a numerical method. In present work, Euler method was used.

CHOICE OF C_D-*Re* CORRELATION FOR THIS SYSTEM

While choosing the "best" C_D-*Re* correlation for a system one must be aware of the origins of the correlation. Most of the correlations in the literature were derived by fitting constants to experimental data. Not all investigators have provided a theoretical evidence or proof to justify their agreement with experimental data. Also, this agreement with experimental data should be reproducible at different experimental conditions. Table 2.1 in Chapter II lists some of the C_D-*Re* correlations reported.

For the current work, the correlation suggested by Concha and Almendra (1979) is selected for predicting the drag coefficient. This expression is based on a formula suggested by Abraham (1970) as a "heuristic argument." The expression suggested has the following form:

$$C_D = C_0\left[1 + \frac{\delta_0}{Re^{1/2}}\right]^2 \tag{3.11}$$

In equation 3.11, C_0 is a parameter derived from Stokes law and δ_0 is the boundary layer thickness parameter such that $\delta_0/ (Re)^{1/2} = 2\delta/d_p$ where δ is the boundary layer thickness of a sphere. In Stokes region, that is for $Re<<1$, Equation 3.11 reduces to Stokes law ($C_D=24/Re$) due to the functional dependence $C_0 \delta_0^2=24$ as per Abraham's expression. A value of 9.06 is suggested for δ_0 (Abraham 1970). However, the author himself considers treating δ_0 as an adjustable parameter to fit the experimental data better. Concha and Almendra (1979) used this formula and suggested Equation 3.12.

$$C_D = 0.28\left[1+\frac{9.06}{Re^{1/2}}\right]^2 \tag{3.12}$$

In their expression, Concha and Almendra derive the value of 9.06 from theory and was originally suggested by McDonald (1954). In their theoretical derivation, Concha and Almendra assume that the angle of boundary layer separation for a sphere to be 84°. This value for θ_s is constant for 10,000< Re <150,000 and is calculated from Equation 3.13 suggested by K. Lee (1968).

$$\theta_s = 214\, Re^{-0.1} \tag{3.13}$$

In the present work, the δ_0 value of has been regressed to fit experimental data while the value of C_0 is fixed at 0.28. This made the model a one-parameter model. This avoided regressing both the parameters to fit the experimental data-which would not show how individual operational variables affected the model. Looking at Equation 3.12, it is obvious that C_0 has a direct proportion with the drag coefficient. The sensitivity of the boundary layer thickness parameter (δ_0) is

checked by running the experiments at multiple fluid temperatures, velocities and different particle sizes. The subsequent chapter includes a detailed discussion about this issue.

CHAPTER IV

EXPERIMENTAL METHODS

DESCRIPTION OF EXPERIMENTAL EQUIPMENT

The fundamental aim of this study was to model the bed expansion in an ion exchange unit. The experimental setup and procedures were designed so as to record the bed height as a function of time. A pilot scale mixed bed ion exchange plant was used for this purpose. The unit consists of three transparent plastic columns one each for cation regeneration, anion regeneration and resin storage. Each column has an inner diameter of 0.3048 m and is 3.5 m tall. A 440V centrifugal pump supplies water to the beds from a large feed tank. A thermostat heater controls the temperature of the water in the feed tank. Transfer of water to the column can be done either from the top or bottom depending on the desired flowpath. Introducing water from the bottom of the bed is called 'backwashing' the resin bed. Each column can be operated in isolation using the valves on the inlet and outlet lines. The cation regeneration column has six ports to transfer resin after separation. Air supply is available to pressurize the columns to drain the water out of the column. Vent valves are provided at the top of each column for depressurization. The cation resin used was DOWEX 650C while the anion

resin was DOWEX 550A. Figure 4.1 is a schematic of the ion exchange plant unit.

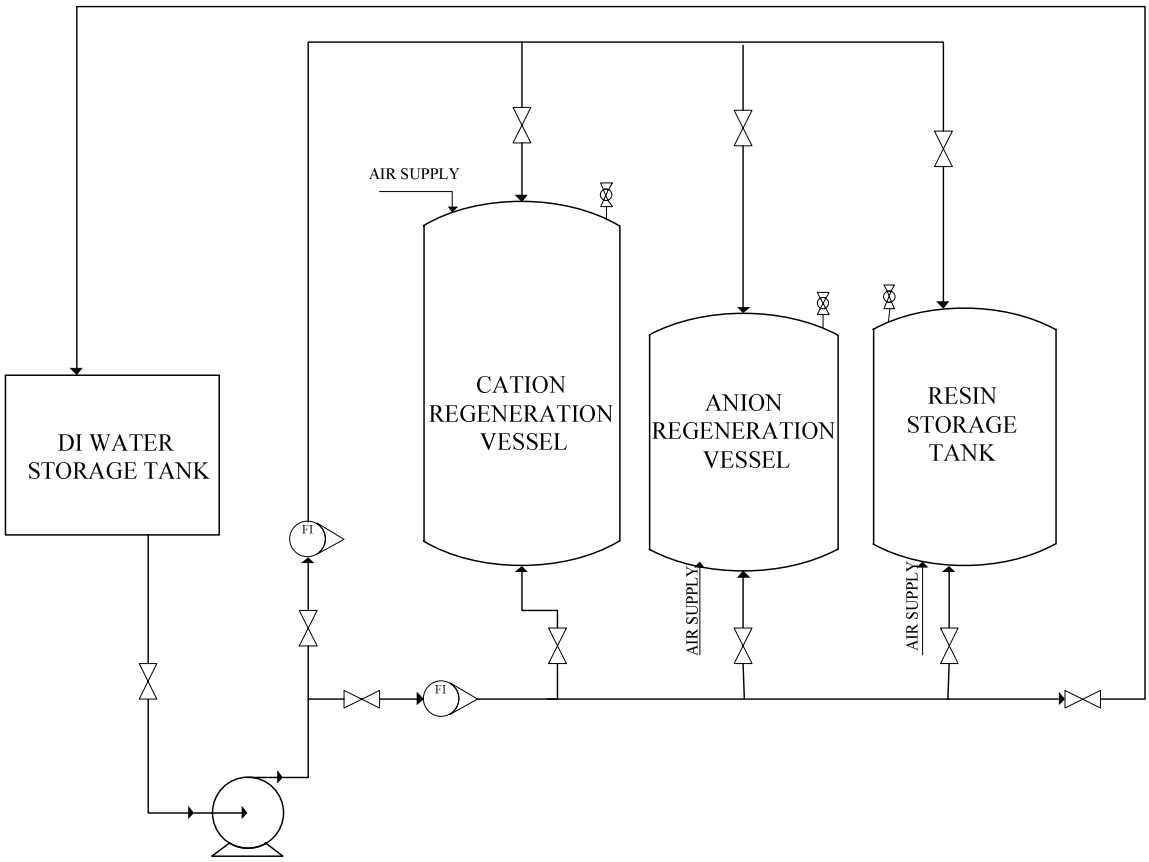

Figure 4.1. Schematic of ion exchange unit

EXPERIMENTAL PROCEDURE

Preliminary tasks of the unit included checking the level of water in the reservoir, inspecting piping and fittings for leaks, checking the temperature of the reservoir water and checking the pressure gauge on the air supply for adequate pressure. The cation and anion resins were separated prior to the backwash operation. This was done by separating the resins using consecutive backwashes. In a single backwash, the bed was allowed to expand to the desired height and

allowed to settle by shutting off the pump. The resin particles settled under the effect of gravity. Once the bed settled, the water used for backwash had to be transferred back to the storage tank. The water was drained from the column by opening the drain valve. By closing the vent valve the column was pressurized with air which pushed the water in the bed through the drain valve back to the storage tank. After consecutive backwashes, the anion and cation resins separate due to the density difference. Once a clear separation of resins was achieved, the bed was fluidized at a low flow rate (to keep the resin layers intact) and the lighter anion resin layer was transferred to the anion storage vessel through the transfer ports.

Once the resins were separated, the flow rate for the experiment was adjusted manually by the supply valve at the inlet of the flow meter. Once the desired flow rate was achieved, three backwashes were done for that particular flow rate at the set temperature. The flow rate adjustment for the cation and anion columns was similar. Note that while draining water out of the column prior to each run, the water level was kept slightly above the bed surface. This ensured that the bed was completely submerged and ensured constant bed porosity at start up. A partially submerged bed did not expand uniformly.

Three flow rates were chosen by visual inspection of the cation bed expansion. At a flow rate higher than 17 gpm, the column overflowed from the top before the bed expanded to a steady fluidized state. Since this state was important from the modeling perspective, three flow rates were chosen so that the cation bed would achieve the steady fluidized conditions. The flow rates chosen

were 17 gpm (high flow condition), 13 gpm (medium flow condition) and 5 gpm (low flow condition). The experiments were batch operation rather than continuous. This was because, for a continuous operation, at lower flow rate condition (5 gpm) the head offered by the water in the entire bed was too much for the pump to operate against. This resulted in an unsteady flow at the low flow rate.

Backwash cycles for the anion column proved challenging. This was because, unlike the cation column (which has air supply at the top and bottom), the anion column has air supply only at the bottom. This prolonged the draining of the column. Another difficulty was obtaining a flat bed surface in the anion column due to agitation during draining. Additionally, at the onset of backwash, there was considerable turbulence which made the initial bed height readings difficult to record.

Assuming the bed surface as a datum, markings were made on the outside surface of the column to record the bed height. The non-fluidized height of the cation bed was 0.45m and that of the anion bed was 0.4 m. A digital video recorder was used to record the backwash expansion for every run. The video was later replayed on a computer for data acquisition. During playback, the time at which the pump was turned on was set as time zero. Each experiment was repeated three times to allow for calculation of experimental errors. The time required for the bed to reach each distinct marked height was recorded as a data point. In data regression, the model parameter was regressed to minimize squared deviations of the model with data from all three runs.

Using the thermostat heater in the storage tank, the temperature of water was adjusted. Changing the temperature required recycling the water through the piping while the heating element was turned on. This ensured uniform heating inside the tank. The temperature of water at ambient conditions was found to be 23^{o}C. Additional temperature set points used were: 30^{o}C, 35^{o}C, 40^{o}C and 45^{o}C. This change in temperature allowed change in fluid properties of density and dynamic viscosity to be variables for analysis of bed expansion phenomena. The values for density and viscosity of water at the three temperatures were obtained from literature (Wakeham 1978).

Experiments for the anion bed were done at 5 and 17 gpm (low and high flow rates) and 23^{o}C and 40^{o}C (low and high temperatures). These conditions were chosen because the purpose of using anion particles was to investigate the effect of particle size (diameter) on the model performance.

From the column geometry, the superficial velocity of water u was calculated by diving the flow rate by the cross-sectional are of the column. Table 4.1 shows the calculated superficial velocities at the three flow rates.

Table 4.1. Calculated superficial velocities at different flow rates

Flow Rate, gpm	Calculated superficial velocity, u, m/s
5	0.00431
13	0.011
17	0.014

CHAPTER V

RESULTS AND DISCUSSION

Figure 5.1 illustrates the experimental data collected for cation resin bed expansion at 23°C (ambient temperature) for the three flow rates. It is a plot of the bed height recorded at different time instances. At time t = 0 the particle velocity, u_p, is zero. At this time instant, the relative velocity of the particle (u_f - u_p) is very high. Since the drag force is proportional to the square of the relative velocity, F_D on the particle is also high. At the onset of fluidization due to a high drag force the bed expands rapidly as the particle velocity approaches the fluid velocity. As the particle velocity comes close to the fluid velocity, the relative velocity reduces causing the drag force on the particle to diminish and it reaches a minimum. After this point, the particle steadily decelerates causing a slow increase in its relative velocity and thus the drag force. The bed as a result approaches a steady fluidized condition and stops expanding. This phenomenon is graphically represented in Figure 5.1. The slope of the expansion profile reduces progressively and levels off towards the end representing a steady state fluidized condition. The error bars for the data points in Figure 5.1 are horizontal

representing the standard deviation in the experimental measurement of the time values at the respective heights.

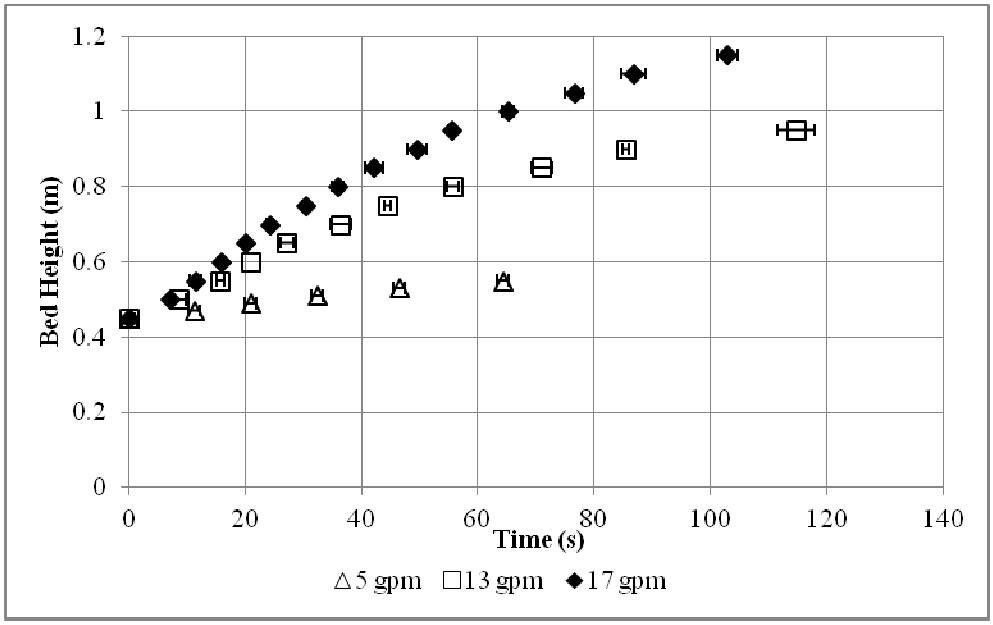

Figure 5.1. Expansion of cation resin bed at 23°C

As discussed in Chapter III, Equation 3.11 was chosen as the drag correlation for this work, where, C_0 value was 0.28 and the parameter δ_0 was regressed to fit the experimental data. The data were regressed to reduce the sum of squared deviation of the model. The data collected for the medium flow rate condition (13 gpm) for the cation resin (d_p = 0.00065 m) at 23°C were used and the regressed value of δ_0 was found to be 5.5.

$$C_D = C_0\left[1+\frac{\delta_0}{Re^{1/2}}\right]^2 \tag{3.11}$$

Figure 5.2 compares the model prediction with the experimental data after regression. In this figure, the solid line is a locus of instantaneous heights

calculated from Equations 3.8 and 3.9 which is an initial value problem with boundary conditions of $u_p = 0$, $h = 0.45$ at $t = 0$ for cation bed and $u_p = 0$, $h = 0.4$ at $t = 0$ for the anion bed. The solution also gave instantaneous values for C_D, Re, du_p/dt and ε. The Reynolds number is calculated from the instantaneous relative velocity of the particle. Due to the porosity function $f(\varepsilon)$ described in Equation 3.10, the model accounts for the change in the bed porosity during expansion. The bed porosity for each time instant was calculated from the height prediction of the previous time instant. The porosity of the bed in the packed condition was assumed to be 0.35. The measure of the model deviation for a particular set of data points is reported as percent average absolute deviation (%AAD). The %AAD values reported henceforth are based on all the data collected for that particular case. Equations 5.1a and 5.1b were used for %AAD calculation where n was the number of data points for that case.

$$\%Deviation = \frac{Estimated - Experimental}{Experimental} x100 \tag{5.1a}$$

$$\%AAD = \frac{1}{n}\sum \left|\%Deviation\right| \tag{5.1b}$$

The model showed excellent agreement with the experimental data with an AAD of 2.78%. The model tends to over predict the bed height at lower time values (on set of fluidization).

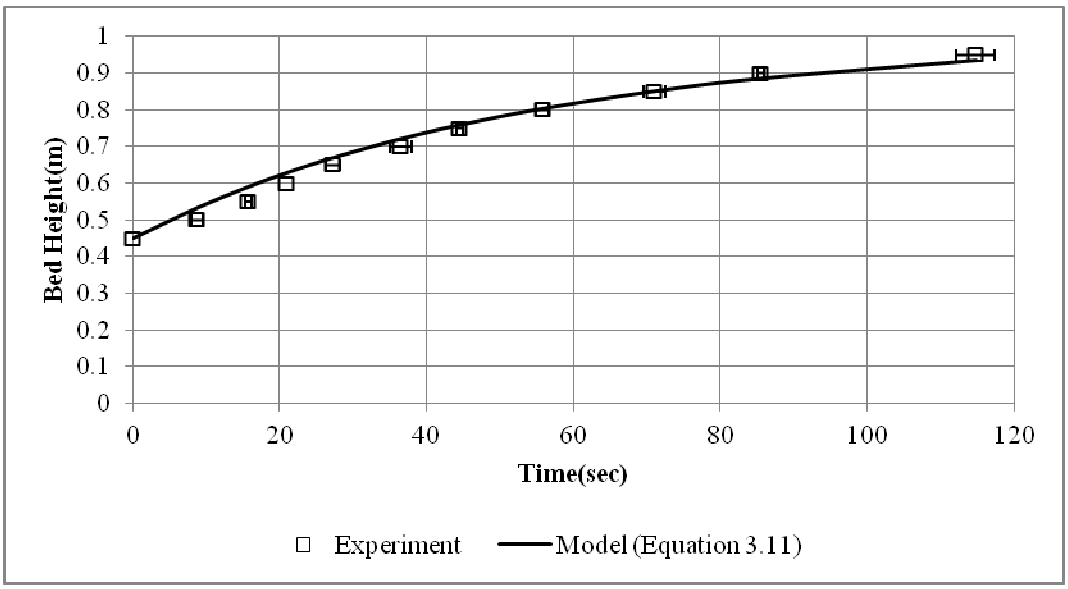

Figure 5.2. Model performance at 13 gpm and 23°C

For the low flow rate condition (5 gpm), the model over predicts the bed height with an AAD of 4.86% for the same δ_0 value of 5.5 and at 17 gpm, the model under predicts the expanded bed height with an AAD of 3.82%. Such a behavior of the model can be expected for the two extremes as the value of δ_0 used for these cases was regressed for the medium flow rate. Since boundary layer thickness is a function of Reynolds number, the 'best' value of δ_0 (a function of boundary layer) will change with velocity. Abraham (1970) presented a relation (Equation 5.2) between the boundary layer, δ, radius of the particle, r, the boundary layer thickness parameter, δ_0 and the Reynolds number, Re. Figures 5.3 and 5.4 illustrate the model performance at 5 and 17 gpm respectively with the δ_0 value of 5.5.

$$\frac{\delta}{r} = \frac{\delta_0}{Re^{1/2}} \tag{5.2}$$

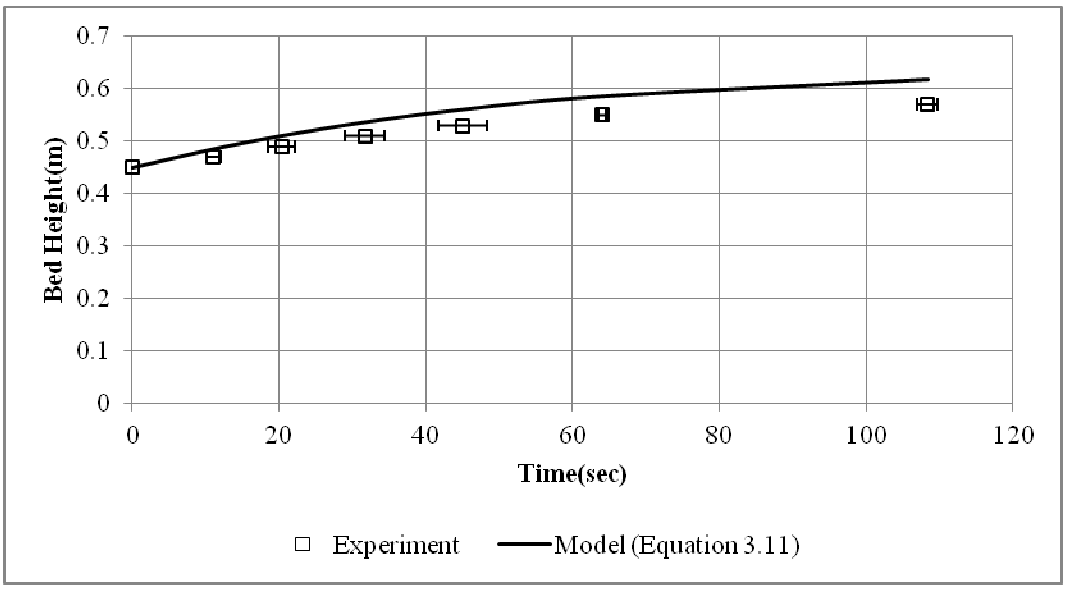

Figure 5.3. Model performance at 5 gpm and 23°C (δ_0 = 5.5)

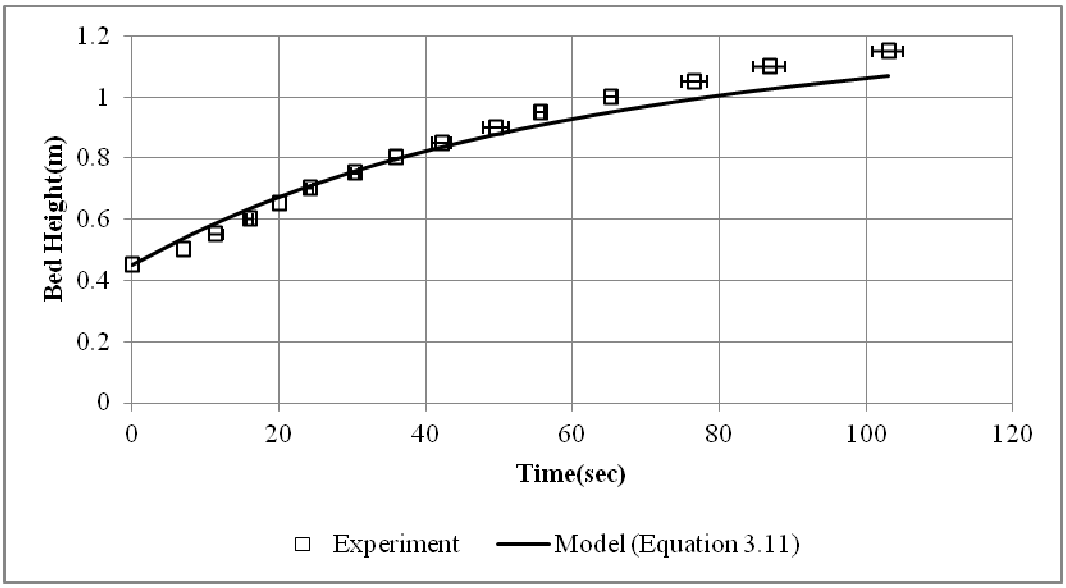

Figure 5.4. Model performance at 17 gpm at 23°C (δ_0 = 5.5)

Figures 5.2 through 5.4 compare the model performance at the three flow rates. The model follows a linear path at lower time values i.e. at the onset of fluidization. The trend of over-prediction of height at lower time values is

observed in all three flow rates. This can be attributed to the fact that the flow rate at $t = 0$ was not the set flow rate. There was a delay in the system to reach the set flow rate. Thus at the lower time values, the actual fluid flow rate is much lower than the set flow rate. The model however assumes that the fluid flow rate and thus the velocity are constant from the onset of fluidization.

EFFECT OF SUPERFICIAL VELOCITY ON MODEL PERFORMANCE

To check for the effect of superficial flow velocity (flow rate) of water on δ_0, the regressed δ_0 values were found for the experimental data at 5 and 17 gpm backwash flow rates. Rearranging Equation 5.2,

$$\frac{2\delta}{d_p} = \delta_0 \sqrt{\frac{\mu}{\rho d_p u}}$$

Separating and rearranging,

$$\delta_0 = 2\delta \sqrt{\frac{u\rho}{d_p \mu}} \tag{5.3}$$

Equation 5.3 suggests a direct proportionality relation between δ_0 and the superficial velocity u. Table 5.1 shows that the regressed δ_0 values increase with the velocity and confirms this relation. This relationship between δ_0 and u is helpful in terms of understanding the model sensitivity to a flow rate change. By understanding this dependence of δ_0 on u, the model can predict bed expansion more accurately. Additionally, this also explains the deviation at the higher and lower flow rates for a δ_0 value found at the medium flow condition. A power law fit of the data reveals the power of u to be 0.39, which is different from the

theoretical power number of 0.5 as in Equation 5.3. The deviation from the theoretical power number (0.5) can be attributed to the fact that the boundary layer thickness, δ, is inversely proportional to the Reynolds number and thus the velocity. Additionally, the theoretical relation in Equation 5.3 assumes a constant velocity (flow rate). In reality, the flow rate during operation fluctuated around the set flow rate. These fluctuations can be attributed to a variable head offered by the water column in the bed. Furthermore, on starting the pump, it took some time to achieve the set flow rate. For instance, it takes twelve seconds for the backwash flow rate to reach 13 gpm. While regressing δ_0 these non-idealities were not accounted for.

Table 5.1. Comparison of regressed δ_0 values for different flow rates at 23°C

Flow Rate, gpm	Calculated Velocity, m/s	Regressed value of δ_0	%AAD in bed height prediction
5	0.00431	4	1.18
13	0.011	5.5	2.78
17	0.014	6.5	2.67

EFFECT OF WATER TEMPERATURE ON MODEL PERFORMANCE

To check for the effect of water temperature on the parameter δ_0, the model was tested with the experimental data collected for the cation bed with 13 gpm backwash flow rate at 30, 35, 40 and 45°C. The change in density of water at these temperatures was negligible when compared to the change in viscosity.

Initially, the value used for δ_0 was 5.5 for this comparison. At 23°C and 13 gpm for the cation resin, the model had an AAD value of 2.78%. Figures 5.5 through 5.8 illustrate the model performance for the cation resin (13 gpm) at 30°C and 40°C respectively.

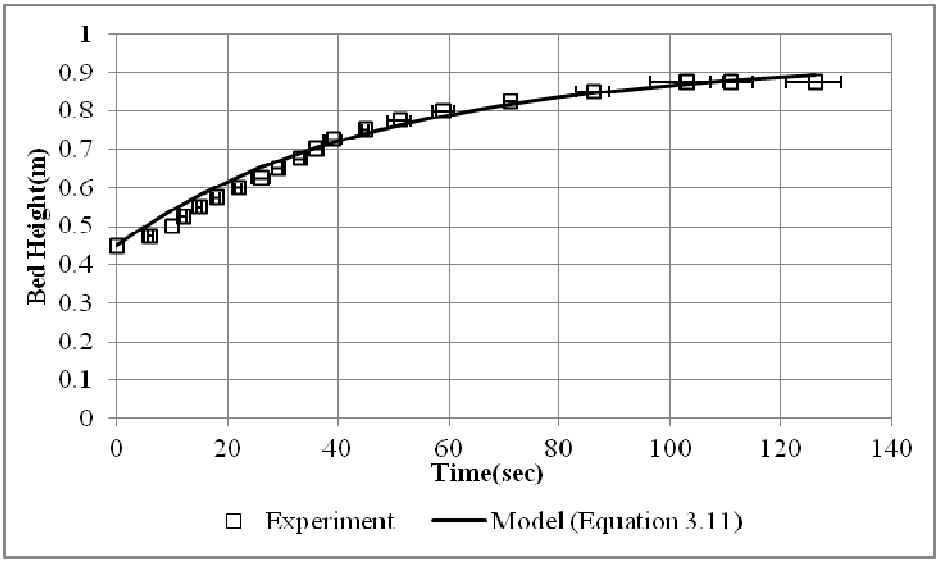

Figure 5.5. Model performance at 13 gpm at 30°C (δ_0 = 5.5)

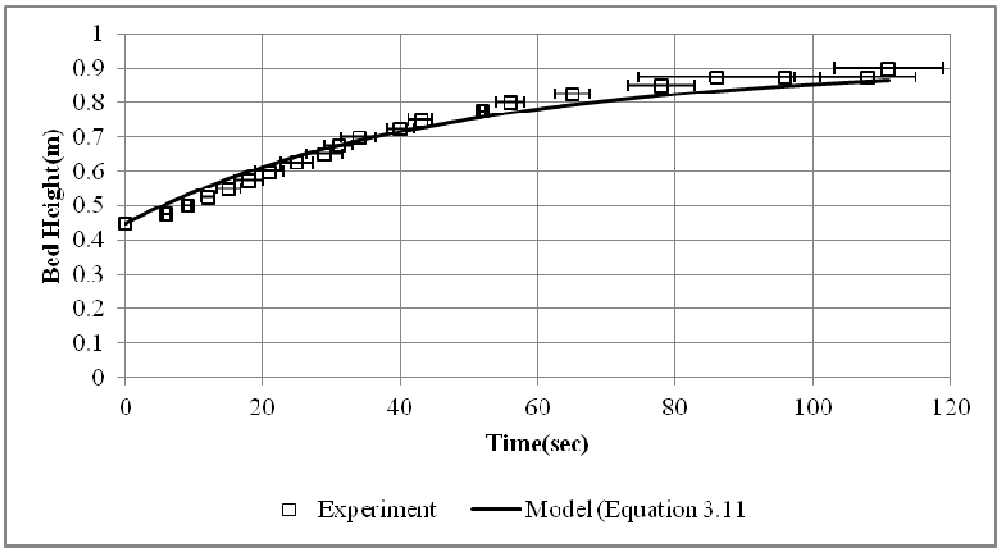

Figure 5.6. Model performance at 13 gpm at 35°C (δ_0 = 5.5)

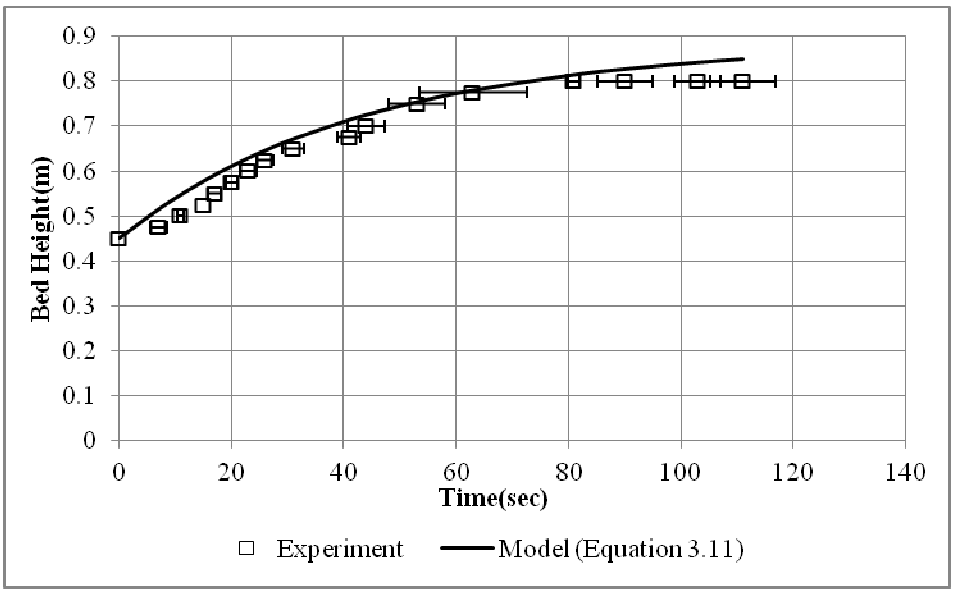

Figure 5.7. Model performance at 13 gpm at 40°C (δ_0 = 5.5)

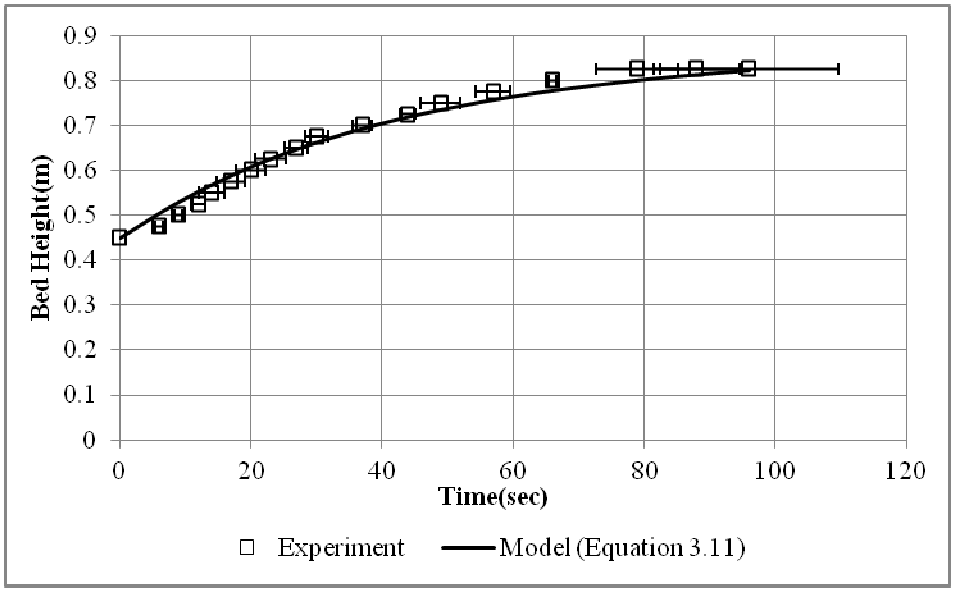

Figure 5.8. Model performance at 13 gpm at 45°C (δ_0 = 5.5)

In Figures 5.2 and 5.5 through 5.8 it should be noted that the steady state expansion heights from the experiments varied with temperatures. The expanded bed height changed from 0.95 cm at 23°C to 0.825 cm at 45°C. This can be

explained by the decrease in fluid viscosity resulting in a decrease in the viscous drag force on the particles. As a result the bed expanded to a lower height at elevated temperatures.

At 30°C, the model predicts the bed expansion profile with an AAD value of 3.08%. The regressed δ_0 values were found to be close to 5.5 at all temperatures. Table 5.2 shows the AAD values for the model prediction for different temperatures with a δ_0 value of 5.5. Although there is a 40% decrease in water viscosity at 45°C there was a small change in the AAD values for different temperatures using the same δ_0. This shows that viscosity of the fluid has very little effect on δ_0 till 45°C. Such a relation between δ_0 and μ can be explained from Equation 5.3. In the equation, the boundary layer thickness δ of the sphere is proportional to the square root of the kinematic viscosity of the fluid (Schlichting 1979). This would cancel out the viscosity and density terms from the Reynolds number making δ_0 independent of μ. Although theoretically δ_0 is independent of μ, experiments suggest a slight change in δ_0 values with temperature. This observation is important as it eliminates temperature as an major contributing factor in choosing the 'best' δ_0 value.

Table 5.2. Comparison of model performance values for 13 gpm at different temperatures (δ_0 = 5.5)

Temperature, °C	Viscosity of water, Ns/m^2	%AAD in bed height prediction
23	0.00102	2.78
30	0.000798	3.08
35	0.000719	3.08
40	0.000653	6.06
45	0.000596	3.71

EFFECT OF PARTICLE SIZE ON MODEL PERFORMANCE

In order to investigate the effect of particle size on δ_0 and ultimately on the model performance, similar experiments were performed using the anion resins (d_p = 0.00059 m). Data for 5, 13 and 17 gpm was recorded for the anion resin at 23°C and 40°C. It should be noted that at 13 and 17 gpm flow rates, the anion bed did not reach a steady fluidized condition due to overflow of water from the top. For all three flow conditions there was turbulence at the onset of fluidization due to which there was no clear interface. This made it impossible to take time readings at lower time values. Experiments showed that the anion particles rose much higher and faster due to their smaller diameters and lesser densities. Figure 5.9 shows the experimental data collected for the anion experiments for the two flow rates at 23°C.

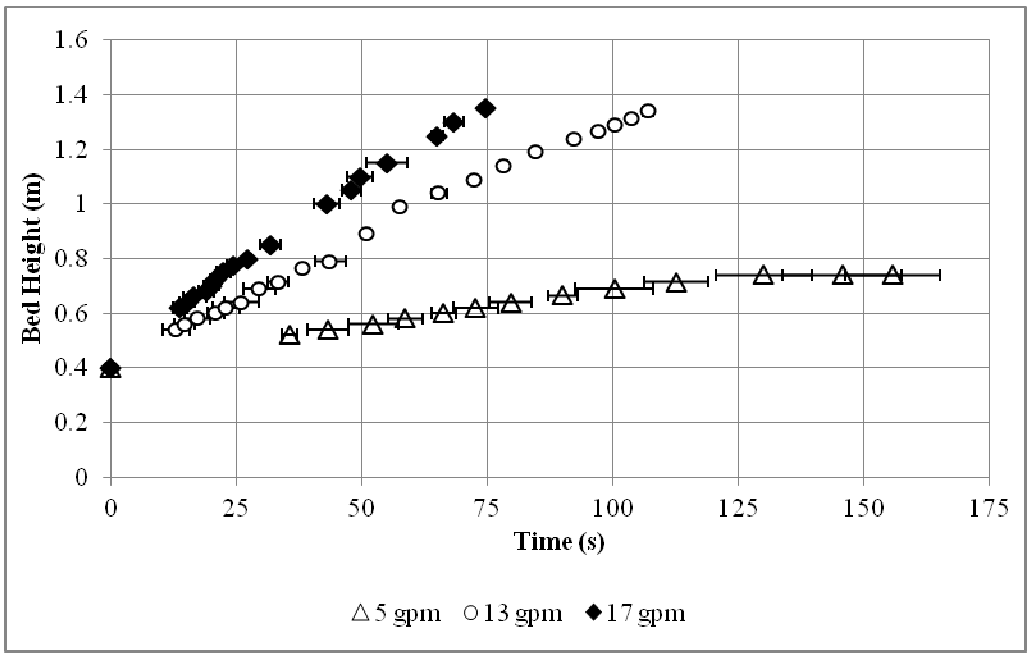

Figure 5.9. Expansion of anion resin bed at 23°C

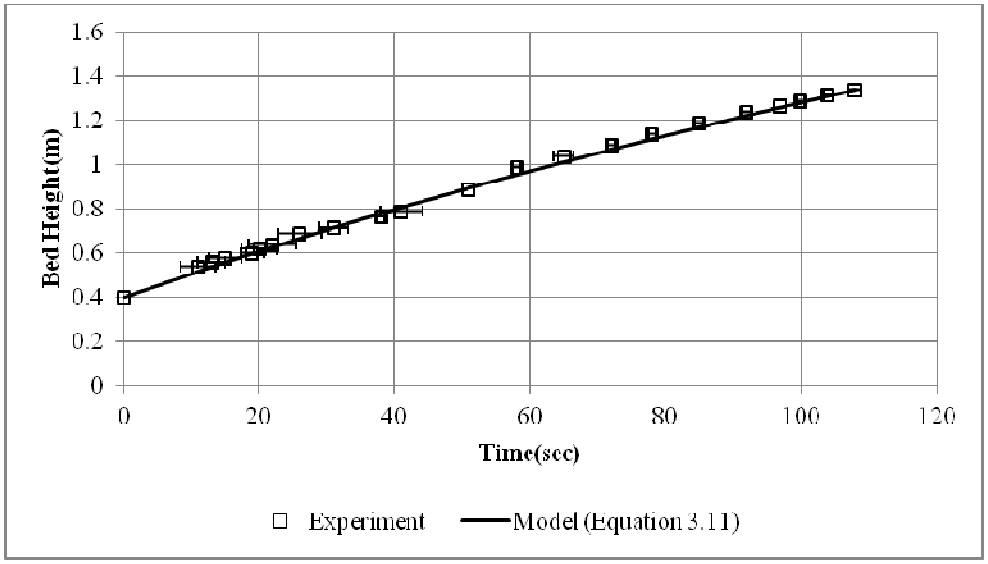

Figure 5.10. Model performance for anion 13 gpm at 23°C (δ_0 = 9.2)

The regressed δ_0 values for 13 gpm experiments at 23°C for both the type of resins were compared. Figure 5.8 shows the model performance for the anion

resin with a regressed δ_0 value of 9.2. Although the anion bed did not reach a steady fluidized condition like the cations, the model predicts the expansion profile vey accurately with an AAD value of 2.47%. Table 5.3 shows a comparison of regressed δ_0 values for the two resin types. Change in particle diameter increases the value of δ_0 to achieve an accurate model prediction. The inverse relation between δ_0 and d_p in Equation 5.3 is confirmed by the experiments. Since difference in particle size is one of the contributing factors in resin separation mixed bed ion exchange (other is particle density), this dependence of δ_0 on d_p will account for the change in particle size for the to resins.

Table 5.3. Effect of particle size on the value of δ_0 at 13 gpm backwash

Type of resin	Particle diameter, d_p, m	Regressed value of δ_0	%AAD in bed height prediction
Cation	0.00065	5.5	2.78
Anion	0.00059	9.2	2.47

COMPARISON OF MODEL PERFORMANCE WITH DIFFERENT C_D-Re CORRELATIONS

For the present study, a formula suggested in the literature (Equation 3.11) was used to fit the model to the experimental data. The effect of the operational variables (velocity, temperature and particle size) on δ_0 was studied. It is,

however, important to compare these 'best fit' adjustments in the model with the correlations reported in the literature. Figure 5.8 shows a comparison of the performance of the model with two correlations for the cation resin at 23°C and 13 gpm backwash flow rate. The figure shows that the model with a value of 5.5 for the parameter δ_0 in Equation 3.11gives the most accurate prediction of bed expansion at this condition due to regression with the experimental data. Stokes law and the correlation by Concha and Almendra (1979) based on Equation 3.11 over predict the expanded bed.

The δ_0 value assumed by Concha and Almendra is based on an angle of separation of boundary layer (θ_s) value of 84°. This θ_s value is constant for 10,000< *Re* <150,000 and can be calculated from Equation 3.13. In present work, calculated particle *Re* values are considerably lower ($0 < Re < 15$). This range is much close to Stokes range ($Re \leq 1$) and this explains better performance of Stokes Law. Table 5.4 shows the comparison of AAD of the model from the experimental data using different C_D-*Re* correlations.

Table 5.4 Comparison of model performance using different C_D-*Re* correlations for cation resin (13 gpm, 23°C)

C_D-*Re* Correlation used	%AAD in bed height prediction
Present work (δ_0=5.5)	2.614
Stokes law	7.322
Concha and Almendra	10.01

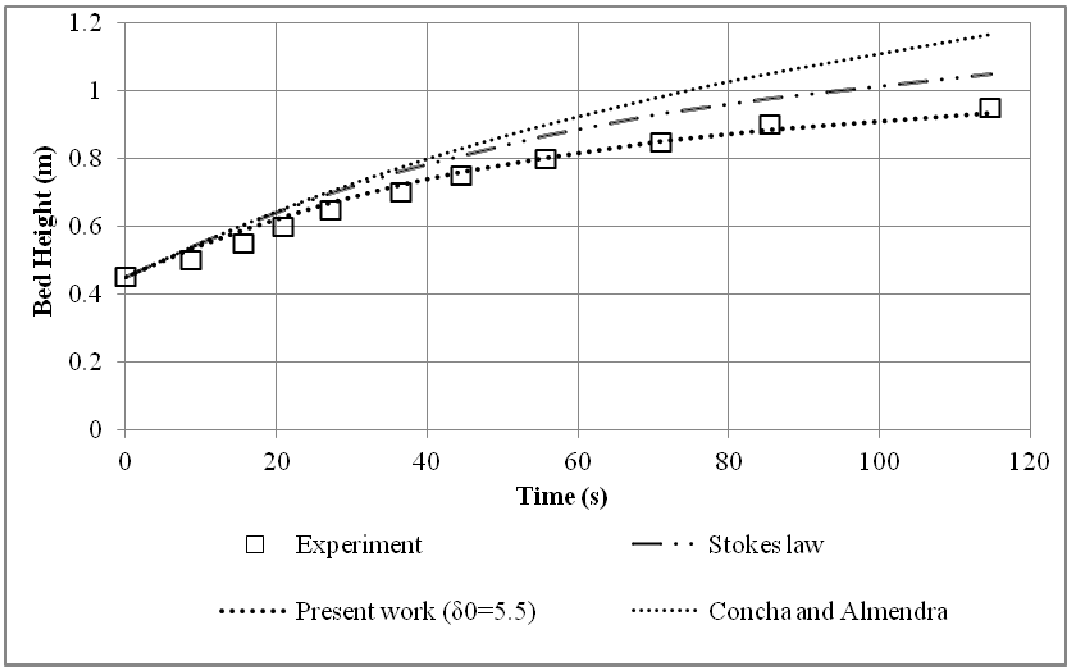

Figure 5.11. Comparison of model performance using different CD-Re correlations (13 gpm, 23°C)

CONCLUSIONS AND RECOMMENDATIONS

This work investigated the phenomenon of bed expansion by studying the phenomenon of particle rise. A model was developed to predict the height of expanded bed. This model accounted for the physical properties of the particle as well as the fluid. By choosing a reported semi-empirical C_D-*Re* relation, it was adjusted for the experimental data. To check for any functional dependence of the adjustable parameter δ_0 on the operational variables (velocity, temperature and particle size), experiments were repeated at different conditions. Experiments revealed that backwashing at different conditions resulted in varied bed expansion. The suggested model predicted the bed height as a function of time accurately. It was observed that the parameter δ_0 was independently related to each of these variables. A theoretically based expression (Equation 5.3) represents the theoretical relationship of these operational variables with δ_0. Equation 5.4 shows the functional relationship between δ_0 and the operational variables. The parameter δ_0 had a direct proportion with fluid velocity, u, viscosity μ (although very slight) and an inverse relation with particle diameter d_p.

$$\delta_0 = f\left(u, \frac{1}{d_p}, \mu\right) \tag{5.4}$$

Possible future work includes finding exact power relations of δ_0 with all the operational variables. This will need more experimental data. By running experiments at higher flow rates the dependence of δ_0 with u can be studied in detail. Similarly, using cation and anion resins of different sizes (diameters),

effect of d_p on δ_0 can be studied. By combining the proposed bead rise model with a bead fall model such as the one suggested by Gopalakrishnan (2011), separation of two resins in backwash can be predicted. Additionally, running experiments at more temperatures, viscosity effects can be recorded. The recommended maximum operating temperature for anion resins in the industry is 60^{o}C (Elmiger 1989). Also, running with the two resins mixed in different proportions can reveal valuable information about cross contamination at different flow rates and temperatures.

Furthermore, additional experiments will help in making the model more robust for different ion exchange systems. A robust model can help an equipment designer avoid over designing of the unit. But correctly predicting the bed expansion height and known flow rates and for known quantities of resin, optimal transfer port locations can be found for a column of given height. Additionally, an operator can predict the accurate height of the fluidized bed for a fixed bed expansion.

REFERENCES

Abraham, F. F. (1970). "Functional Dependence of Drag Coefficient of a Sphere on Reynolds Number." Phys. Fluids **13**(2194).

Schlichting, H. (1979). "Boundary Layer Theory." 128.

Wakeham, J. K. M. S. W. A. (1978). "Viscosity of liquid water in the range -8 Deg. C to 150 Deg. C." J. Phys. Chem. Ref. Data **7**(3): 941.

Abraham, F. F. (1970). "Functional Dependence of Drag Coefficient of a Sphere on Reynolds Number." Phys. Fluids **13**(2194).

Concha, F. and E. R. Almendra (1979). "Settling velocities of particulate systems, 1. Settling velocities of individual spherical particles." International Journal of Mineral Processing **5**(4): 349-367.

K. Lee, H. B. (1968). "Transport process in flow around a sphere with particular reference to the transfer of mass." Int. J. Heat Mass Transfer **11**: 1020.

Lapple, C. E. and C. B. Shepherd (1940). "Calculation of particle trajectories." Industrial & Engineering Chemistry **32**(5): 605-617.

McDonald, J. E. (1954). "THE SHAPE AND AERODYNAMICS OF LARGE RAINDROPS." Journal of Meteorology **11**(6): 478-494.

Richardson, J. F. and W. N. Zaki (1954). "Sedimentation and fluidization. I." Trans. Inst. Chem. Eng. **32**(Copyright (C) 2012 American Chemical Society (ACS). All Rights Reserved.): 35-53.

Ruckenstein, E. (1964). "Homogeneous Fluidization." Industrial & Engineering Chemistry Fundamentals **3**(3): 260-268.

Yang, J. and A. Renken (2003). "A generalized correlation for equilibrium of forces in liquid–solid fluidized beds." Chemical Engineering Journal **92**(1–3): 7-14.

Brodkey, R. S. (1967). The phenomena of fluid motions. Reading, Mass., Addison-Wesley Pub. Co.**:** xiv, 737 p.

Concha, F. and E. R. Almendra (1979). "Settling velocities of particulate systems, 1. Settling velocities of individual spherical particles." International Journal of Mineral Processing **5**(4): 349-367.

Courdec, J. P. (1985). Incipient fluidization and particulate systems. Fluidization. R. C. J.F Davidson, D. Harrison. London, Academic Press**:** 1–46.

Dharmarajah, A. H. and J. L. Cleasby (1986). "Predicting the expansion behavior of filter media." J. - Am. Water Works Assoc. **78**(Copyright (C) 2012 American Chemical Society (ACS). All Rights Reserved.): 66-76.

Didwania, A. K. and G. M. Homsy (1981). "Flow regimes and flow transitions in liquid fluidized beds." International Journal of Multiphase Flow **7**(6): 563-580.

Flemmer, R. L. C. and C. L. Banks (1986). "On the drag coefficient of a sphere." Powder Technology **48**(3): 217-221.

Haider, A. and O. Levenspiel (1988). "Drag Coefficient and Terminal Velocity of Spherical and Nonspherical Particles." Powder Technology **58**: 64.

J. B. Romero, L. N. J. (1962). "Factors affecting fluidized bed quality." Chemical Engineering Progress; Symposium Series **58**: 28-37.

Karamanev, D. G. (1996). "Equations for calculation of the terminal velocity and drag coefficient of solid spheres and gas bubbles." Chemical Engineering Communications **147**: 75-84.

Kelbaliyev, G. I. (2011). "Drag coefficients of variously shaped solid particles, drops, and bubbles." Theoretical Foundations of Chemical Engineering **45**(3): 248-266.

Khan, A. R. and J. F. Richardson (1987). "THE RESISTANCE TO MOTION OF A SOLID SPHERE IN A FLUID." Chemical Engineering Communications **62**(1-6): 135-150.

Kwauk, R. H. W. a. M. (1948). "Fluidization of Solid Particles." Chemical Engineering Progress **44**(3).

Lapple, C. E. (1951). Particle Dynamics. Wilmington, Delaware, E.I Dupont de Nemours and co.

Lewis, E. W. and E. W. Bowerman (1952). "Fluidization of solid particles in liquids." Chem. Eng. Prog. **48**(Copyright (C) 2012 American Chemical Society (ACS). All Rights Reserved.): 603-610.

Mabrouk, R., J. Chaouki, et al. (2007). "Effective drag coefficient investigation in the acceleration zone of an upward gas–solid flow." Chemical Engineering Science **62**(1–2): 318-327.

Massey, B. S. (1968). Mechanics of fluids. London, Van Nostrand.

Oseen, C. W. (1911). Arkiv. Mat. Astron. Fysik **6**(29).

Richardson, J. F. and W. N. Zaki (1954). "Sedimentation and fluidization. I." Trans. Inst. Chem. Eng. **32**(Copyright (C) 2012 American Chemical Society (ACS). All Rights Reserved.): 35-53.

Schiller, L. and A. Naumann (1933). "Über die grundlegenden berechungen bei der schwerkraftaufbereitung." Vereines Deutscher Ingenieure **77**: 318.

Sholji, I. (1987). "Expansion of granular filters during backwash." Journal of Environmental Engineering **113**(3): 516-531.

Stokes, G. G. (1851). Trans. Cambridge Phil. Soc **9**: 8.

Wen, C. Y. and Y. H. Yu (1966). "Mechanics of fluidization." Chem. Eng. Prog., Symp. Ser. **62**(Copyright (C) 2012 American Chemical Society (ACS). All Rights Reserved.): 100-111.

Yang, J. and A. Renken (2003). "A generalized correlation for equilibrium of forces in liquid–solid fluidized beds." Chemical Engineering Journal **92**(1–3): 7-14.

Helfferich, F. (1995). Ion Exchange, Dover Publications.

Kunin, R. and F. X. McGarvey (1951). "Monobed Deionization with Ion Exchange Resins." Industrial & Engineering Chemistry **43**(3): 734-740.

Owens, D. L. (1995). Practical Principles of Ion Exchange Water Treatment, Tall Oaks Publishing Inc.

APPENDIX A

EXPERIMENTAL RESULTS

Table A.1. Cation bed with 5 gpm backwash flow at 23°C

Bed Height, m	Time, s		
	Run 1	Run 2	Run 3
0.45	0	0	0
0.47	10	11	12
0.49	20	22	19
0.51	34	32	29
0.53	44	47	44
0.55	64	64	64
0.57	110	107	108

Table A.2. Cation bed with 13 gpm backwash flow at 23°C

Bed Height, m	Time, s		
	Run 1	Run 2	Run 3
0.45	0	0	0
0.5	9	10	8
0.55	15	16	16
0.6	21	21	21
0.65	27	29	27
0.7	35	38	35
0.75	44	45	44
0.8	56	57	55
0.85	70	73	70
0.9	85	86	85
0.95	111	116	117

Table A.3. Cation bed with 17 gpm backwash flow at 23°C

Bed Height, m	Time, s		
	Run 1	Run 2	Run 3
0.45	0	0	0
0.5	7	7	7
0.55	10	11	12
0.6	15	16	16
0.65	20	20	20
0.7	24	25	24
0.75	30	31	30
0.8	37	36	35
0.85	44	41	43
0.9	50	47	50
0.95	55	55	56
1	65	66	64
1.05	77	79	76
1.1	87	90	86
1.15	102	105	105

Table A.4. Cation bed with 5 gpm backwash flow at 30°C

Bed Height, m	Time, s		
	Run 1	Run 2	Run 3
0.45	0	0	0
0.47	8	9	10
0.49	13	20	16
0.51	18	34	22
0.53	31	54	34
0.53	52	85	55
0.53	62	98	79
0.53	72	114	98
0.53	95	124	110

Table A.5. Cation bed with 13 gpm backwash flow at 30°C

Bed Height, m	Time, s		
	Run 1	Run 2	Run 3
0.45	0	0	0
0.475	6	7	7
0.5	10	10	10
0.525	12	13	12
0.55	15	16	16
0.575	18	18	19
0.6	22	22	23
0.625	26	28	29
0.65	29	30	31
0.675	33	32	34
0.7	36	38	38
0.725	39	41	42
0.75	45	45	46
0.775	51	54	50
0.8	59	61	57
0.825	71	71	69
0.85	86	88	82
0.875	103	108	95
0.875	111	117	110
0.875	126	127	118

Table A.6. Cation bed with 17 gpm backwash flow at 30°C

Bed Height, m	Time, s		
	Run 1	Run 2	Run 3
0.45	0	0	0
0.475	6	6	6
0.5	8	8	7
0.525	10	11	10
0.55	12	13	12
0.575	14	15	14
0.6	16	17	16
0.625	18	19	18
0.65	21	22	19
0.675	24	24	22
0.7	25	26	26
0.725	27	29	27
0.75	30	31	30
0.775	33	33	32
0.8	36	36	34
0.825	40	39	37
0.85	44	43	38
0.875	48	48	44
0.925	58	61	52
1.05	94	89	82
1.075	104	100	90
1.1	110	108	96
1.125	129	123	110
1.125	135	125	116

Table A.7. Cation bed with 13 gpm backwash flow at 35°C

Bed Height, m	Time, s		
	Run 1	Run 2	Run 3
0.45	0	0	0
0.475	6	7	6
0.5	9	10	9
0.525	12	13	11
0.55	15	15	12
0.575	18	19	15
0.6	21	22	18
0.625	25	25	21
0.65	29	30	25
0.675	31	33	29
0.7	34	37	32
0.725	40	42	38
0.75	43	46	43
0.775	52	51	51
0.8	56	60	59
0.825	65	70	68
0.85	78	86	87
0.875	86	107	104
0.875	96	115	115
0.875	108	120	120
0.9	111	123	126

Table A.8. Cation bed with 13 gpm backwash flow at 45°C

Bed Height, m	Time, s		
	Run 1	Run 2	Run 3
0.45	0	0	0
0.475	6	7	7
0.5	9	10	10
0.525	12	12	14
0.55	14	16	18
0.575	17	20	21
0.6	20	24	24
0.625	23	27	27
0.65	27	30	30
0.675	30	33	33
0.7	37	39	40
0.725	44	46	46
0.75	49	52	55
0.775	57	58	62
0.8	66	66	67
0.825	79	88	91
0.825	88	95	101
0.825	96	102	122

Table A.9. Cation bed with 5 gpm backwash flow at 40°C

Bed Height, m	Time, s		
	Run 1	Run 2	Run 3
0.45	0	0	0
0.47	21	26	28
0.49	55	42	45
0.51	104	82	85
0.51	119	98	102
0.51	128	104	107

Table A.10. Cation bed with 13 gpm backwash flow at 40°C

Bed Height, m	Time, s		
	Run 1	Run 2	Run 3
0.45	0	0	0
0.475	10	9	7
0.5	12	12	11
0.525	15	15	15
0.55	19	17	17
0.575	22	21	20
0.6	25	26	23
0.625	28	29	26
0.65	35	33	31
0.675	42	45	41
0.7	50	49	44
0.75	62	54	53
0.775	78	60	63
0.8	82	80	81
0.8	98	99	90
0.8	111	108	103
0.8	121	121	111

Table A.11. Cation bed with 17 gpm backwash flow at 40°C

Bed Height, m	Time, s		
	Run 1	Run 2	Run 3
0.45	0	0	0
0.025	2	6	6
0.05	4	7	8
0.075	7	9	11
0.1	9	11	13
0.125	11	13	14
0.15	13	16	16
0.175	16	18	19
0.2	19	20	21
0.25	25	22	25
0.275	29	24	29
0.3	34	28	33
0.35	40	36	39
0.375	43	43	45
0.4	48	49	51
0.45	60	58	64
0.475	67	69	68
0.5	74	76	76
0.525	83	85	84
0.55	96	97	94
0.55	102	106	98
0.55	107	111	106

Table A.12. Anion bed with 5 gpm backwash flow at 23°C

Bed Height, m	Time, s		
	Run 1	Run 2	Run 3
0.4	0	0	0
0.54	39	43	44
0.56	47	52	53
0.58	55	58.5	59
0.6	64	66.5	66
0.62	68	72.5	73
0.64	75	79	81
0.66	87	90	90
0.68	94	101.5	98
0.7	109	114.5	109
0.725	119	119	134
0.75	132	142.5	152
0.75	140	149	158

Table A.13. Anion bed with 13 gpm backwash flow at 23°C

Bed Height, m	Time, s		
	Run 1	Run 2	Run 3
0.4	0	0	0
0.54	11	16	12
0.56	13	17	14
0.58	15	20	17
0.6	19	22	22
0.62	20	24	25
0.64	22	28	28
0.69	26	32	31
0.715	31	34	35
0.765	38	38	39
0.79	41	43	47
0.89	51	51	51
0.99	58	58	57
1.04	65	67	64
1.09	72	72	73
1.14	78	79	78
1.19	85	84	85
1.24	92	92	93
1.265	97	97	97
1.29	100	100	101
1.315	104	103	104
1.34	108	106	107

Table A.14. Anion bed with 17 gpm backwash flow at 23°C

Bed Height, m	Time, s		
	Run 1	Run 2	Run 3
0.62	14	15	17
0.64	15	16	18
0.66	17	17	21
0.68	19	20	22
0.7	20	21	23
0.725	23	23	25
0.75	24	25	27
0.775	26	26	28
0.8	29	29	30
0.85	31	34	35
1	41	43	46
1.05	47	49	51
1.1	49	51	54
1.15	55	55	62
1.25	65	65	67
1.3	69	67	71
1.35	75	75	75

Table A.15. Anion bed with 5 gpm backwash flow at 40°C

Bed Height, m	Time, s		
	Run 1	Run 2	Run 3
0.4	0	0	0
0.54	38	46	33
0.56	47	50	39
0.58	58	55	60
0.6	66	65	69
0.62	72	73	79
0.64	82	84	96
0.66	86	91	109
0.68	101	104	113
0.7	113	121	129
0.725	126	166	166
0.75	153	219	195
0.775	173	240	260
0.775	217	250	272

Table A.16. Anion bed with 17 gpm backwash flow at 40°C

Bed Height, m	Time, s		
	Run 1	Run 2	Run 3
0.4	0	0	0
0.5	8	10	9
0.54	13	11	11
0.56	15	12	12
0.58	16	14	13
0.6	17	16	15
0.62	18	17	17
0.64	19	19	19
0.66	21	21	21
0.7	27	25	24
0.8	32	30	30
0.85	34	34	37
0.925	43	43	46
0.95	46	45	48
1	51	47	51
1.05	55	51	54
1.1	58	55	56
1.15	60	57	59
1.2	63	67	65
1.25	72	71	70
1.3	77	77	75
1.35	83	82	79

VITA

Sanket Kulkarni

Candidate for the Degree of

Master of Science

Thesis: PREDICTING ION EXCHANGE BEAD RISE DURING BACKWASH FLOW

Major Field: Chemical Engineering

Biographical:

Education:

Received Bachelor of Chemical Engineering for University of Pune, 2007

Received Master of Science in Chemical Engineering at Oklahoma State University, 2012

Experience:

Worked as a Process Engineer at Praxair India Pvt. Ltd. in Bangalore India from August 2007 to December 2008

Worked as a Teaching and Research Assistant at the School of Chemical Engineering, Oklahoma State University from August 2010 to June 2012.

Name: Sanket Kulkarni Date of Degree: July, 2012

Institution: Oklahoma State University Location: Stillwater, Oklahoma

Title of Study: PREDICTING ION EXCHANGE BEAD RISE DURING BACKWASH FLOW

Pages in Study: 66 Candidate for the Degree of Master of Science

Major Field: Chemical Engineering

Scope and Method of Study:

Separation of cationic and anionic resin is an important step in mixed bed ion exchange operation. Prior to regeneration good separation of the two resins reduces cross contamination. Inefficient separation of the resins also leads to loss of capacity. By accurately predicting the height of the resin interface, the separation of the resins can be improved. This study proposes a bed expansion model that accurately predicts the bed expansion height.

Findings and Conclusions:

The proposed model accurately predicts the expansion of an ion exchange bed. Experiments showed that the model parameter δ_0 was a function of the fluid temperature, fluid flow rate and the resin particle diameter. A functional relationship between the model parameter and the operational was established.

ADVISER'S APPROVAL: Dr. Gary L. Foutch